NAL OF GEOPHYSICAL RESEARCH
Solid Earth
AN AGU JOURNAL

JGR

Volume 119 • Issue 11 • November 2014 • Pages 7993–8576

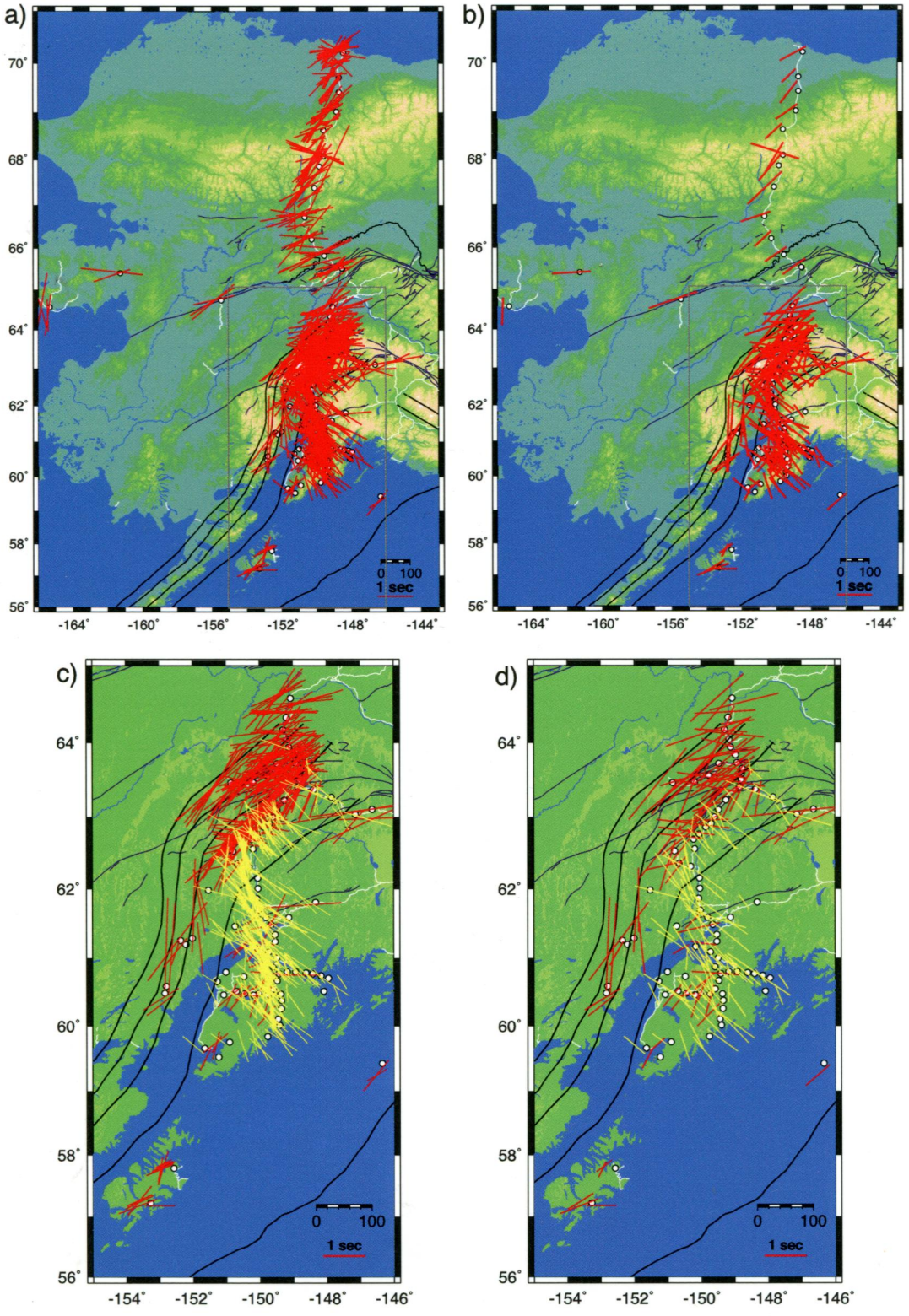

AGU PUBLICATIONS

WILEY

Journal of Geophysical Research Solid Earth

Volume 119 Issue 11 November 2014
JGREA2(11) 7993–8576 (2014)
ISSN 2169-9313 (print); ISSN 2169-9356 (Online)

The online article is the official version and may contain additional content not available in this print issue. To access the full article, including multimedia, enhanced figures, supporting information, and other nonprinted content, go to http://wileyonlinelibrary.com/journal/jgrb.

Geomagnetism and Paleomagnetism/Marine Geology and Geophysics

7993 *Eric Font, Cristina Veiga-Pires, Manuel Pozo, Claire Carvallo, António Carlos de Siqueira Neto, Pierre Camps, Sébastien Fabre, and José Mirão*
Magnetic fingerprint of southern Portuguese speleothems and implications for paleomagnetism and environmental magnetism (doi 10.1002/2014JB011381)

8021 *M. Muraoka, M. Ohtake, N. Susuki, Y. Yamamoto, K. Suzuki, and T. Tsuji*
Thermal properties of methane hydrate-bearing sediments and surrounding mud recovered from Nankai Trough wells (doi 10.1002/2014JB011324)

Chemistry and Physics of Minerals and Rocks/Volcanology

8034 *Anna M. Dymshits, Konstantin D. Litasov, Igor S. Sharygin, Anton Shatskiy, Eiji Ohtani, Akio Suzuki, and Kenichi Funakoshi*
Thermal equation of state of majoritic knorringite and its significance for continental upper mantle (doi 10.1002/2014JB011194)

8047 *Xi Zhang, Andrew P. Bunger, and Robert G. Jeffrey*
Mechanics of two interacting magma-driven fractures: A numerical study (doi 10.1002/2014JB011273)

8064 *Shaocheng Ji, Tongbin Shao, Matthew H. Salisbury, Shengsi Sun, Katsuyoshi Michibayashi, Weihua Zhao, Changxing Long, Fenghua Liang, and Takako Satsukawa*
Plagioclase preferred orientation and induced seismic anisotropy in mafic igneous rocks (doi 10.1002/2014JB011352)

8089 *Toshihiko Shimamoto and Hiroyuki Noda*
A friction to flow constitutive law and its application to a 2-D modeling of earthquakes (doi 10.1002/2014JB011170)

8107 *B. P. Proctor, T. M. Mitchell, G. Hirth, D. Goldsby, F. Zorzi, J. D. Platt, and G. Di Toro*
Dynamic weakening of serpentinite gouges and bare surfaces at seismic slip rates (doi 10.1002/2014JB011057)

8132 *Julie Richard, Jean-Pierre Gratier, Mai-Linh Doan, Anne-Marie Boullier, and François Renard*
Rock and mineral transformations in a fault zone leading to permanent creep: Interactions between brittle and viscous mechanisms in the San Andreas Fault (doi 10.1002/2014JB011489)

8154 *E. S. G. Rainey and A. Kavner*
Peak scaling method to measure temperatures in the laser-heated diamond anvil cell and application to the thermal conductivity of MgO (doi 10.1002/2014JB011267)

Seismology

8171 *Suguru Yabe and Satoshi Ide*
Spatial distribution of seismic energy rate of tectonic tremors in subduction zones (doi 10.1002/2014JB011383)

8186 *Aditya Riadi Gusman, Yuichiro Tanioka, Breanyn T. MacInnes, and Hiroaki Tsushima*
A methodology for near-field tsunami inundation forecasting: Application to the 2011 Tohoku tsunami (doi 10.1002/ 2014JB010958)

8207 *Jean Baptiste Tary, Mirko van der Baan, Bruce Sutherland, and David W. Eaton*
Characteristics of fluid-induced resonances observed during microseismic monitoring (doi 10.1002/2014JB011263)

8223 *L. De Siena, C. Thomas, G. P. Waite, S. C. Moran, and S. Klemme*
Attenuation and scattering tomography of the deep plumbing systemof Mount St. Helens (doi 10.1002/2014JB011372)

8239 *Jeanne L. Hardebeck*
The impact of static stress change, dynamic stress change, and the background stress on aftershock focal mechanisms (doi 10.1002/2014JB011533)

8267 *Joanna E. Hamlyn, Derek Keir, Tim J. Wright, Jürgen W. Neuberg, Berhe Goitom, James O. S. Hammond, Carolina Pagli, Clive Oppenheimer, J-Michael Kendall, and Raphaël Grandin*
Seismicity and subsidence following the 2011 Nabro eruption, Eritrea: Insights into the plumbing system of an off-rift volcano (doi 10.1002/2014JB011395)

8283 *Luigi Improta, Pasquale De Gori, and Claudio Chiarabba*
New insights into crustal structure, Cenozoic magmatism, CO_2 degassing, and seismogenesis in the southern Apennines and Irpinia region from local earthquake tomography (doi 10.1002/2013JB010890)

0148-0227JB-119-11

8312 *Nadav Wetzler, Amir Sagy, and Shmuel Marco*
The association of micro-earthquake clusters with mapped faults in the Dead Sea basin (doi 10.1002/2013JB010877)

8331 *Chao Liu, Andrea Bizzarri, and Shamita Das*
Progression of spontaneous in-plane shear faults from sub-Rayleigh to compressional wave rupture speeds (doi 10.1002/2014JB011187)

8346 *S. Pachhai, H. Tkalčić, and J. Dettmer*
Bayesian inference for ultralow velocity zones in the Earth's lowermost mantle: Complex ULVZ beneath the east of the Philippines (doi 10.1002/2014JB011067)

8366 *Anna Perttu, Douglas Christensen, Geoffrey Abers, and Xiaodong Song*
Insights into mantle structure and flow beneath Alaska based on a decade of observations of shear wave splitting (doi 10.1002/2014JB011359)

8378 *Patricia Martínez-Garzón, Grzegorz Kwiatek, Hiroki Sone, Marco Bohnhoff, Georg Dresen, and Craig Hartline*
Spatiotemporal changes, faulting regimes, and source parameters of induced seismicity: A case study from The Geysers geothermal field (doi 10.1002/2014JB011385)

8397 *H. J. A. Van Avendonk, H. Kuo-Chen, K. D. McIntosh, L. L. Lavier, D. A. Okaya, F. T. Wu, C. Y. Wang, C. S. Lee, and C. S. Liu*
Deep crustal structure of an arc-continent collision: Constraints from seismic traveltimes in central Taiwan and the Philippine Sea (doi 10.1002/2014JB011327)

8417 *B. Shan, J. C. Afonso, Y. Yang, C. J. Grose, Y. Zheng, X. Xiong, and L. Zhou*
The thermochemical structure of the lithosphere and upper mantle beneath south China: Results from multiobservable probabilistic inversion (doi 10.1002/2014JB011412)

8442 *Naofumi Aso and Victor C. Tsai*
Cooling magma model for deep volcanic long-period earthquakes (doi 10.1002/2014JB011180)

8457 *Yosihiko Ogata and Koichi Katsura*
Comparing foreshock characteristics and foreshock forecasting in observed and simulated earthquake catalogs (doi 10.1002/2014JB011250)

8478 *Simanchal Padhy, Takashi Furumura, and Takuto Maeda*
Decoupling of Pacific subduction zone guided waves beneath central Japan: Evidence for thin slab (doi 10.1002/2014JB011562)

Geodesy and Gravity/Tectonophysics

8502 *Tom Parsons, Eric L. Geist, Holly F. Ryan, Homa J. Lee, Peter J. Haeussler, Patrick Lynett, Patrick E. Hart, Ray Sliter, and Emily Roland*
Source and progression of a submarine landslide and tsunami: The 1964 Great Alaska earthquake at Valdez (doi 10.1002/2014JB011514)

8517 *Vasso Saltogianni, Stathis C. Stiros, Andrew V. Newman, Kelly Flanagan, and Fanis Moschas*
Time-space modeling of the dynamics of Santorini volcano (Greece) during the 2011–2012 unrest (doi 10.1002/2014JB011409)

8538 *Bradford J. Foley, David Bercovici, and Linda T. Elkins-Tanton*
Initiation of plate tectonics from post-magma ocean thermochemical convection (doi 10.1002/2014JB011121)

8562 *Carolina Pagli, Hua Wang, Tim J. Wright, Eric Calais, and Elias Lewi*
Current plate boundary deformation of the Afar rift from a 3-D velocity field inversion of InSAR and GPS (doi 10.1002/2014JB011391)

Cover. In *Christensen et al.* [DOI: 10.1002/2014JB011359], image shows SKS wave splitting results for stations on Figure 1. The red lines are parallel to the fast splitting direction, and the length of each line is proportional to the splitting time (δt). Splitting observations are plotted at the 100 km projection of the ray paths to unravel back azimuth behavior of the measurements. Wadati-Benioff zone contours (black lines) are plotted at the trench and 50, 100, 150, and 200 km depths. Shown are (a) all individual results and (b) back azimuth bin-averaged values as discussed in text. In the ARCTIC experiment, all measurements at each station were averaged due to the consistent behavior at all back azimuths (except for station CHS). (c and d) Same as Figures 4a and 4b but enlarging detail for Southern Alaska; splitting bars are color coded such that yellow bars denote splitting directions within 45° of plate motion and red bars denote other splitting directions. Gray boxes on Figures 4a and 4b show regions covered on Figures 4c and 4d. See pp. 8366-8377.